A Novel Data-Driven Current Control Design for Grid-Connected Inverter with LCL Filter

Muhammad Usama, Thomas Chevet, Nicolas Langlois

A Novel Data-Driven Current Control Design for Grid-Connected Inverter with LCL Filter

Muhammad Usama
Université de Rouen Normandie,
ESIGELEC, IRSEEM,
76000 Rouen, France
muhammad.usama@esigelec.fr

Thomas Chevet
Université de Rouen Normandie,
ESIGELEC, IRSEEM,
76000 Rouen, France
thomas.chevet@esigelec.fr

Nicolas Langlois
Université de Rouen Normandie,
ESIGELEC, IRSEEM,
76000 Rouen, France
nicolas.langlois@esigelec.fr

***Abstract*—This paper presents a novel current control approach for grid-connected inverters employing deep symbolic regression (DSR). The proposed control approach overcomes the limitations of traditional proportional-integral (PI) controllers. Although PI controllers are commonly used due to their simple structure, their practical implementation in real-world grid-connected inverter applications presents computational challenges. Precise gain tuning, real-time integral computation, and additional anti-windup mechanisms significantly increase execution time, particularly in high-speed digital control systems, making them less efficient for applications requiring fast dynamic response and reduced computational complexity. By replacing the conventional PI controller with DSR-based current control, we significantly reduce computational burden and improve adaptability under varied operating conditions. In addition, the proposed controller addresses the decoupling inaccuracies commonly encountered in the conventional PI-based control approach. DSR works offline to provide numerical analytical expressions that give optimal control performance. The simulation results demonstrate that the DSR-based current control gives better steady-state performance and lower harmonic distortion compared to the conventional PI current control. The test results validate the effectiveness of the proposed control scheme, highlighting its potential to improve power quality and operational robustness in practical grid applications, making it a promising alternative for efficient grid-connected inverter control.**

***Index Terms*—Grid-connected inverter, analytical expressions, deep symbolic optimization, computational complexity**

I. Introduction

The evolution of decentralized and renewable energy sources has encouraged the swift adoption of microgrids, power systems capable of operating autonomously or in coordination with the main power grid [1]. Microgrids offer flexibility and environmental benefits by integrating sources such as solar photovoltaic (PV), wind, and battery storage systems. In particular, grid-connected inverters play a vital role in synchronizing distributed energy resources with the main grid, guaranteeing stable power flow and maintaining power quality [2]. The control of these inverters is crucial as they are responsible for maintaining voltage stability, minimizing harmonic distortion, and handling variable power generation. Among numerous configurations, LCL-filtered inverters have gained popularity in grid-connected applications due to their ability to attenuate high-frequency switching harmonics effectively [3]. However, the control of LCL-filtered inverters is complex, particularly when grid conditions fluctuate, making it challenging to ensure optimal performance, especially under adversarial disturbances.

Conventional control schemes for LCL-filtered grid-connected inverters are comprised of proportional-integral (PI) or proportional-resonant controllers, which are designed to regulate the current flow and minimize grid-connected inverter errors [4]. While PI controllers are straightforward and commonly used due to their simplicity and ease of implementation, they require careful tuning of gain parameters to ensure stability and optimal performance under different operating conditions. This gain-tuning process can be time-consuming and often requires specialized expertise, hindering flexible deployment in diverse microgrid applications. Furthermore, PI controllers are fundamentally limited in their ability to handle high-order dynamics and disturbances effectively, often resulting in poor performance in the face of grid fluctuations or nonlinearities [5].

To overcome these limitations, numerous advanced control schemes have been studied in the literature, including model predictive control (MPC), adaptive control, and fuzzy logic control, which offer better disturbance rejection and adaptability [6], [7]. However, these schemes cause higher computational complexity, provoke variable switching frequency, and are highly dependent on plant models, making them less suitable for real-world power conversion applications. In addition, the variable switching frequency in the finite control set MPC causes problems in the filter design, resulting in poor inverter control performance and power efficiency [8]. Furthermore, the recent advancement of artificial intelligence (AI) in power electronics has provided promising solutions for adaptive and predictive control. AI-based approaches, such as neural networks and reinforcement learning, have been applied to grid-connected inverter control, providing a degree of flexibility and learning-based adaptation to changing conditions [9], [10]. These methods can offer improvements in terms of robustness and adaptability. However, their implementation is often hindered by substantial computational complexity, as they require considerable resources to train and optimize, particularly

This work was supported by Région Normandie through the PAMAP project.

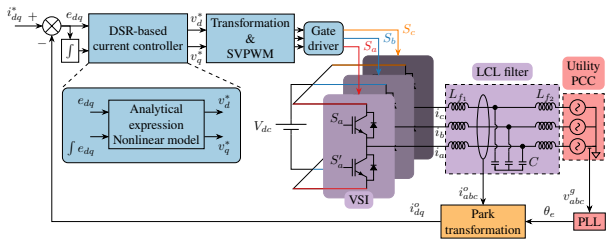

Fig. 1: System model.

in real-time applications. The high computational burden poses a challenge for the implementation of AI-based control solutions in power conversion applications, where real-time response is critical and processing resources may be limited. In addition, the complex calculation, low explainability of neural networks, and local linearization are common concerns that prevent their real-time implementation [11].

To address the limitations of conventional control methods and the computational demands of AI-based approaches, this paper proposes a novel current control scheme that employs deep symbolic regression (DSR) for inverters connected to the filtered LCL grid. Deep symbolic regression (DSR) is a data-driven numerical approach that generates analytical mathematical expressions that represent the underlying patterns in the data [12]. By applying deep symbolic regression, we can achieve a control system that is both adaptable and computationally efficient. Unlike traditional controllers that rely on fixed gain values, the DSR-based approach dynamically derives a nonlinear control law based on the inverter's operational data. This method not only mitigates the gain selection problem but also simplifies the control structure, allowing for fast and efficient execution suitable for power conversion applications [13].

The proposed DSR-based control strategy seeks to maintain the benefits, such as strong disturbance rejection and stability, while reducing the reliance on gain tuning. With the proposed control scheme, the system adapts to variations in operating conditions while avoiding additional computational overhead. In essence, our contribution aims to combine the adaptability and robustness of AI techniques with the efficiency of conventional control systems, leading to a low-complexity, high-performance control strategy for microgrid applications. To the best of our knowledge, this is the first study to design a numerical expression-based current control scheme specifically for AC microgrid applications. The proposed method aims to enable more optimal and efficient control solutions for grid-connected systems.

II. Simulation Model

A. System Model

The system under study is a grid-connected inverter designed for efficient and stable power delivery to the grid. It is assumed that the three-phase grid voltages are balanced and stable, the switches are ideal, and the DC-link voltage is constant. The system model in the dq reference frame is expressed as

$$\begin{bmatrix} v_d \\ v_q \end{bmatrix} = L\frac{d}{dt}\begin{bmatrix} i_d \\ i_q \end{bmatrix} + \begin{bmatrix} r & -\omega L \\ \omega L & r \end{bmatrix}\begin{bmatrix} i_d \\ i_q \end{bmatrix} + \begin{bmatrix} v_{gd} \\ v_{gq} \end{bmatrix} \quad (1)$$

where r is the system's resistance, v_d and v_q are the inverter output voltages, which are influenced by the grid currents i_d and i_q. These currents are affected by the grid voltage components v_{gd} and v_{gq}. The ωL term accounts for the interaction between the grid frequency and the inductive nature of the inverter output filter [14].

The core of the system is the current controller, implemented using DSR, which generates reference voltages based on the desired current tracking requirements as shown in Figure 1. These reference voltages are subsequently fed to a space vector pulse width modulation (SVPWM) unit to determine the appropriate switching signals for the inverter's operation. The inverter is then interfaced with the grid through an LCL filter, which minimizes switching harmonics and ensures compliance with grid standards. The DSR-based controller leverages a data-driven approach to provide optimal reference signals while maintaining robustness under varying operating conditions.

In order to generate data for obtaining the analytic expression of the DSR-based controller, we first run simulations of the system with a conventional PI controller instead of the DSR-based current controller. This PI controller is tuned with gains $K_p = 180$ and $K_i = 0.001$ by trial and error.

B. LCL Filter Design

The design of an LCL filter is integral to ensuring the effective attenuation of switching harmonics in grid-connected inverter systems while maintaining stability and meeting power quality requirements. The structure of the filter is depicted in Figure 1. This paragraph outlines the mathematical basis for the design process, including the calculation of key parameters for LCL filter [15].

1) Resonance Frequency: The resonance frequency f_{res} of the LCL filter is a fundamental design parameter, as it governs the filter's ability to attenuate high-frequency components. It is expressed as

$$f_{\text{res}} = \frac{1}{2\pi}\sqrt{\frac{L_{f_1} + L_{f_2}}{L_{f_1} L_{f_2} C}} \quad (2)$$

where L_{f_1} and L_{f_2} are the inverter-side and grid-side inductances, respectively, and C is the filter capacitance. To avoid interference with the inverter's switching frequency, f_{res} is constrained to be such that $0.2 f_{\text{sw}} \leq f_{\text{res}} \leq 0.5 f_{\text{sw}}$ where f_{sw} is the switching frequency (10 kHz in this study).

2) Filter Capacitance: The filter capacitance C must be chosen to limit the reactive power injected into the grid, defined as $Q_C = \omega C V_{\text{rms}}^2 \leq 0.05 P_{\text{rated}}$ where V_{rms} is the RMS voltage (400 V), $\omega = 2\pi f_{\text{fund}}$ is the angular frequency of the fundamental signal ($f_{\text{fund}} = 50$ Hz), and P_{rated} is the inverter's rated power.

3) Inductance Calculation: The total inductance of the filter $L_{f_{\text{total}}}$ is split between L_{f_1} and L_{f_2} so that $L_{f_{\text{total}}} = L_{f_1} + L_{f_2}$.

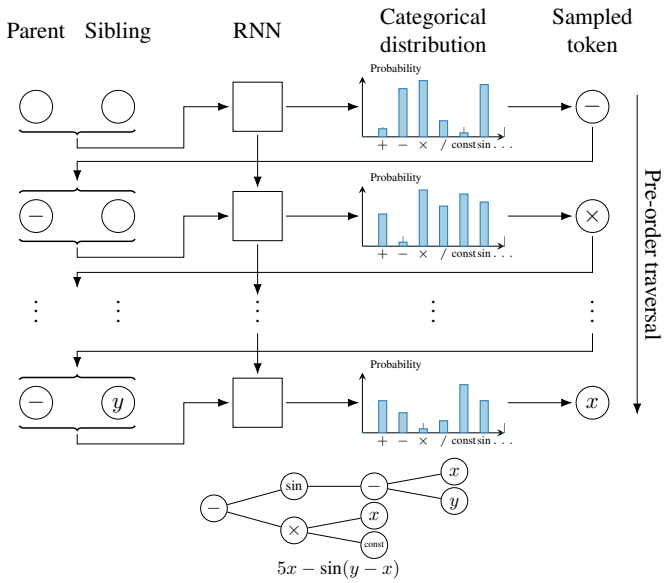

Fig. 2: Generating mathematical expressions with DSR.

Typically, the inverter-side inductance L_{f_1} is set as a fraction k (usually between 0.1 and 0.3) of $L_{f_{\text{total}}}$ such that $L_{f_1} = kL_{f_{\text{total}}}$. However, a higher L_{f_1} effectively lowers the resonance frequency, thereby enhancing system damping and improving current tracking accuracy by attenuating high-frequency switching ripple, leading to enhanced power quality [16]. The grid-side inductance L_{f_2} is then determined accordingly.

4) Stability Criteria: To ensure the stability of the inverter system, the ratio of the inductances must satisfy $L_{f_1} \leq 10L_{f_2}$.

The parameters derived above are selected to balance harmonic attenuation, stability, and system efficiency. This ensures that the grid-connected inverter performs reliably under varying operating conditions.

III. Novel Current Control Scheme

Deep symbolic regression is an advanced approach for symbolic optimization, enabling the extraction of mathematical expressions from empirical data [12]. In this paper, we propose to use DSR offline to obtain an analytic expression of the current controller from simulation data. The method utilizes a given dataset and a predefined token library – i.e., a list of binary operators (e.g., the symbols $+$, $-$, $\times$, $/$, etc.), usual functions (e.g., constants, sin, exp, etc.), and variables representing the input to the controller – and a learning model. This learning model evaluates various possible mathematical expressions defined using elements of the token library and selects the one that best approximates the data distribution [13]. The mathematical expression is represented by an expression tree, an example of which is given in Figure 2.

As presented in [12], a recurrent neural network (RNN) generates a probability distribution in order to sample a token from the library as shown in Figure 2. Tokens are then selected sequentially, with each token's parent and sibling acting as inputs for the RNN to predict the next token in the sequence.

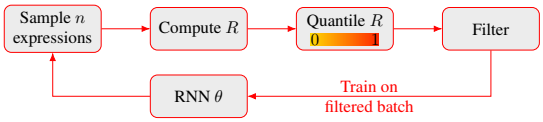

Fig. 3: DSR training flow.

This autoregressive process results in a pre-order traversal of a symbolic tree, which is then reconstructed to form the corresponding expression [17].

Figure 3 illustrates the DSR process. In order to obtain the mathematical expression that best fits the data, the RNN generates, at each step, a batch of candidate expressions sampled from its learned token distribution. The performance of each expression is subsequently assessed using a reward metric, such as the inverse normalized root-mean-squared error (INRMSE), to gauge its fit to the data. Using these rewards, a quantile threshold is implemented to extract the best expressions. These selections, which represent the best candidates, are then used to update the RNN through a training process, enhancing its ability to generate the best expressions in future iterations. This iterative approach ensures a balance between exploring a diverse range of candidate expressions and exploiting those that perform well, leading to the convergence on mathematical models that optimally fit the data.

Each generated expression τ is assigned a reward function $R(\tau)$ to evaluate its quality in fitting the data. In this study, the reward function is based on the INRMSE, calculated as

$$R(\tau) = \frac{\sigma_y}{\sqrt{\frac{1}{n}\sum_{i=1}^{n}\left(y_i - \tau(X_i)\right)^2}} \tag{3}$$

where X_i and y_i, for $i \in \{1, \ldots, n\}$, are sampled input and output data from the dataset and σ_y is the standard deviation of the y_i. In our case, the X_i are the dq-axis current errors and their integrals while the y_i are the dq-axis voltage references provided to the PWM unit.

The error is then computed by comparing the predicted values $\tau(X_i)$ from the candidate expression τ with the true data points y_i. These rewards are then used to adjust the RNN parameters θ using a risk-seeking policy gradient method [12], formulated as

$$J_{\text{risk}}(\theta; \varepsilon) = \mathbb{E}_{\tau \sim p(\tau|\theta)}\left[R(\tau) | R(\tau) \geq R_\varepsilon(\theta)\right] \tag{4}$$

where $R_\varepsilon(\theta)$ is the $(1-\varepsilon)$-quantile of the reward distribution obtained from the policy parameterized by θ. The objective is therefore to maximize the rewards of the top ε samples, ignoring those that fall below a predefined threshold.

As presented in Paragraph II-A, the training data is generated using the model from Figure 1 using a PI controller and the parameters from Table I. The DSR algorithm is run as per Algorithm 1 using the Adam optimizer [18] with $L = 64$ and $N = 2$, and the INRMSE defined in equation (3) as the fitness metric. The considered token library is $\mathcal{T} = \{+, -, \times, /, \text{exponent}, \text{const}, x_1, x_2, x_3, x_4\}$ where x_1 to x_4 represent the input variables to the controller.

Algorithm 1: Deep symbolic regression workflow

Input: training data (X, y), long short-term memory (LSTM) configuration (L, N, optimizer), token library $\mathcal{T} = \{+, -, \times, /, \cos, \sin, \text{const}, \dots\}$, fitness metric R

Output: optimized symbolic expression τ^*

initialize LSTM with L layers, N cells, and chosen optimizer;
do
  generate expressions: sample n candidate expressions τ_i, with $i \in \{1, \dots, n\}$, from LSTM output using the library $\mathcal{T}$;
  for *i from 1 to n* **do**
    evaluate $R(\tau_i)$ with the dataset (X, y);
  end
  filter expressions: select τ_{filtered} for $R(\tau_i) \leq \varepsilon$;
  update LSTM: update LSTM parameters based on τ_{filtered} and chosen optimizer;
while *convergence or max iterations not reached*;

TABLE I: System parameters.

Parameter	Description	Value
f_{fund}	Frequency	$50\,\text{Hz}$
f_{sw}	Switching frequency	$10\,\text{kHz}$
V_{rms}	Grid Voltage	$400\,\text{V}$
L_{f_1}	Inverter-side filter inductor	$0.5\,\text{mH}$
L_{f_2}	Grid-side filter inductor	$0.15\,\text{mH}$
C	Filter capacitor	$0.1\,\mu\text{F}$
R_g	Grid resistance	$1\,\mu\Omega$
L_g	Grid inductance	$1\,\text{pH}$

The optimal analytical expressions for the reference values v_d^* and v_q^*, maximizing the reward and minimizing the decision function, are

$$v_d^* = 1592x_1^3x_3 - x_2^2(-x_1 + x_2x_3(x_1 - x_2)), \quad (5)$$

$$v_q^* = 250x_2(x_1 - 2x_2 + x_3)(x_1 + x_2x_3x_4 - 2x_2 + x_4) \quad (6)$$

where $x_1 = \Delta i_d$, $x_2 = \Delta i_q$, $x_3 = \int \Delta i_d$, and $x_4 = \int \Delta i_q$ respectively. Finally, the derived analytical expressions for the reference voltage (v_{dq}^*) are fed into the space vector pulse width modulation algorithm, which generates the gating pulses for the voltage source inverter.

IV. Test Results

The grid-connected inverter system is simulated in Matlab to evaluate the performance of the proposed data-driven current controller. The system parameters are listed in Table I. A PI controller serves as the benchmark model during the offline training phase. The data-driven controller is trained offline using a laptop equipped with an Intel i7 processor, 32GB RAM, and an NVIDIA RTX 3000 GPU. Figure 1 presents a schematic representation of the data-driven DSR architecture for the grid-connected inverter.

A. Case 1

For the first test case, a constant i_{dq}^* current reference is injected into the system. Figure 4a compares the inverter d-axis current performance between the proposed DSR-based current control method and the conventional PI controller, with respect to the current reference. The results show that the DSR-based controller closely tracks the reference current, presenting close to no deviation over time and a smaller response time, reflecting its effective regulation. In the meantime, the response of the PI controller is slower and oscillatory before stabilizing. For the comparison of q-axis current of the inverter, Figure 4d illustrates the results generated by both methods. Similar to the response for d-axis current, the DSR-based controller shows a more precise tracking of the reference value with less fluctuations or oscillations than the PI controller.

Figure 4e presents grid phase A current and voltage from the results of DSR-based current control, showing near-ideal sinusoidal waveforms, highlighting the proposed method's robustness in regulating both current and voltage, even under changing grid conditions. On the other hand, Figure 4b shows the grid phase A current and voltage obtained with the PI controller having sinusoidal waveforms but with slightly higher distortions than with the DSR-based controller.

The effective performance of the proposed DSR-based current controller is further validated by the lower value of total harmonic distortion (THD) of the phase A of grid current, specifically $0.26\,\%$, in contrast to the conventional methods, as depicted in Figure 4f. Figure 4c is a manifestation of the higher distortions associated with the PI controller, as the grid phase A current's THD with this method is $0.46\,\%$, higher than what is obtained with the proposed controller. This shows that DSR approach achieves better reduction in harmonic distortion and provides higher power quality.

B. Case 2

For further validation of the proposed current control method, a step variation in the i_d^* reference current is introduced to examine the responses of both the DSR-based and PI current controllers. Figure 5a shows that both controllers successfully track the varying reference without significant delay. However, the DSR-based controller demonstrates improved steady-state performance with reduced oscillations and lower steady-state error. In contrast, the PI controller exhibits small deviations around the reference due to its reliance on fixed gain tuning, as shown in Figure 5b.

In order to maintain seamless transitions without significant distortion, the DSR-based current controller ensures that the grid's phase A current effectively tracks the reference current variation with improved performance, as illustrated in Figure 5c. This figure shows that the PI controller demonstrates less precise tracking of the reference current, with visible discrepancies and slightly higher harmonic distortion during the transition, compared to the DSR-based controller. This indicates the inefficiency of the PI controller in maintaining stable current regulation under step variations.

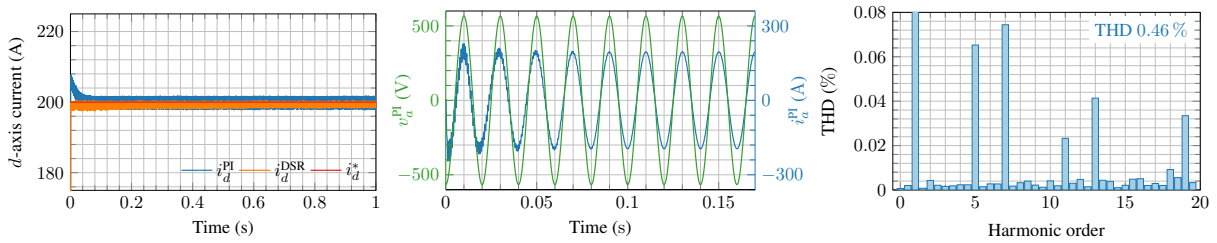

(a) Inverter d-axis current. (b) Grid phase A current and voltage using PI. (c) Harmonic distortion of grid phase A current employing PI.

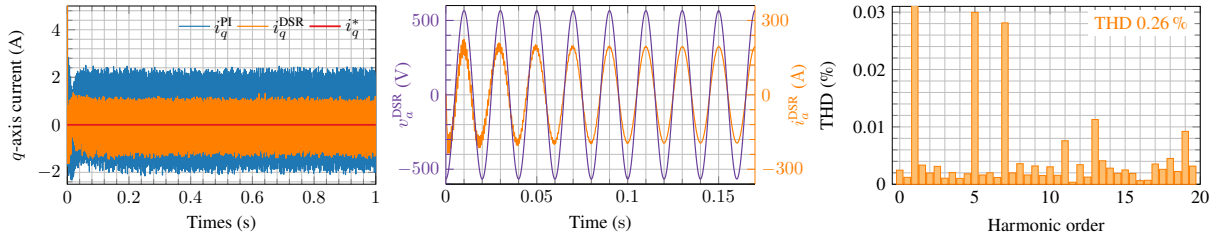

(d) Inverter q-axis current. (e) Grid phase A current and voltage using DSR. (f) Harmonic distortion of grid phase A current employing DSR.

Fig. 4: Grid injected steady-state current using conventional PI and proposed DSR current control.

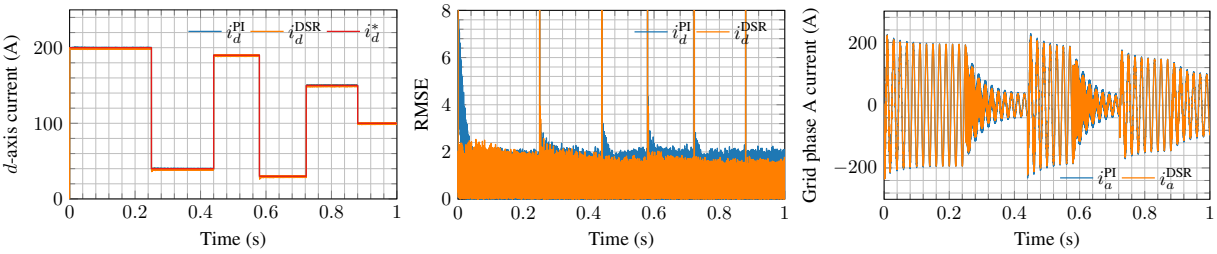

(a) Inverter d-axis current reference variation. (b) Inverter d-axis current RMSE. (c) Grid phase A current response under step change.

Fig. 5: Variation of grid-injected current with conventional PI and proposed DSR current control under varying current reference.

C. Case 3

For the third case, a variation in the i_q^* reactive current is introduced to compare the system's response using the PI and proposed DSR-based controllers. As it can be verified in Figure 6a, both current controllers track the d-axis reference current, but DSR-based controller is more precise with smoother and less oscillatory behavior than the PI controller's response. In addition, the DSR controller tracks the q-axis current variations with high accuracy in Figure 6d, quickly adapting to changes and maintaining a steady-state response with minimal error or fluctuations. On the other hand, the PI controller shows noticeable deviations and oscillations for tracking the q-axis reference current. Figures 6b and 6e present the grid response for current and voltage under the varying reactive current, through the conventional PI and the DSR-based current controller, respectively. The responses in these figures show that the DSR-based controller's response is cleaner than the one delivered by the PI controller, presenting a THD of $0.21\,\%$ compared to the PI controller's $0.43\,\%$, as presented in Figures 6f and 6c, respectively. This shows the proposed DSR-based controller's superiority in maintaining clean current waveform with minimal harmonic distortion, effectively mitigating harmonic interference, which can be particularly beneficial in applications where power quality is critical.

V. Conclusion

This paper proposes a novel current control approach that employs deep symbolic regression (DSR) for AC microgrids, aiming to address the challenges in gain selection, decoupling inaccuracies, and computational complexity common to conventional PI controllers. Leveraging DSR, the control method is adapted to varying grid conditions and disturbances, providing an efficient and straightforward control approach to regulating current in grid-connected systems. The main advantage of the proposed control scheme is the ability to generate a numerical expression that characterizes the data and

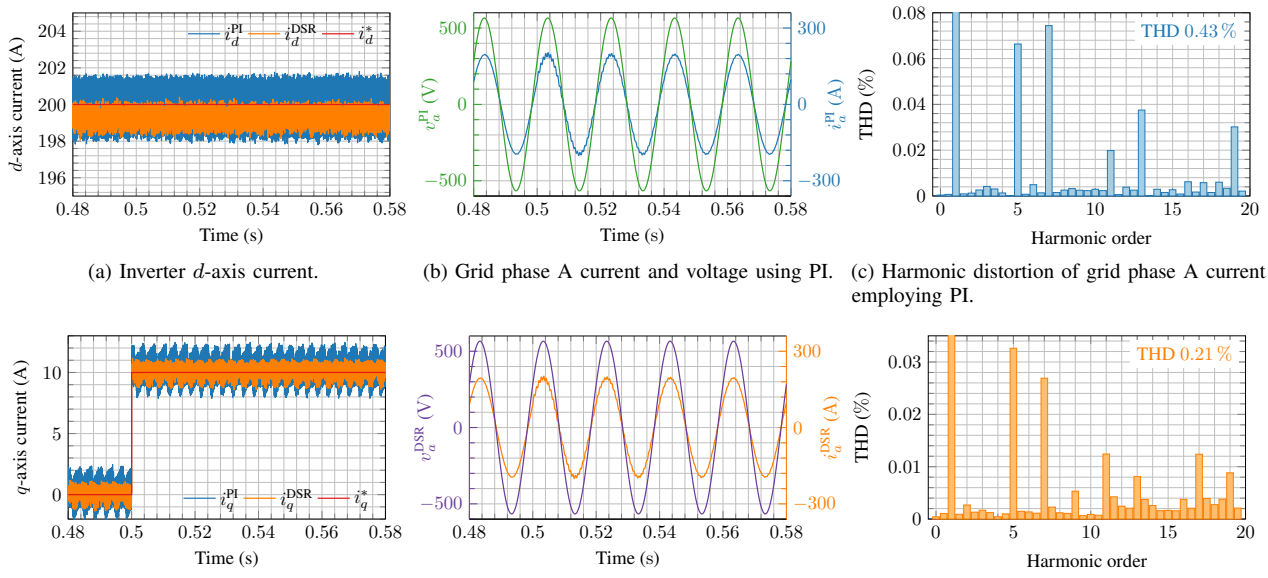

(a) Inverter d-axis current. (b) Grid phase A current and voltage using PI. (c) Harmonic distortion of grid phase A current employing PI.

(d) Inverter q-axis current. (e) Grid phase A current and voltage using DSR. (f) Harmonic distortion of grid phase A current employing DSR.

Fig. 6: Grid injected steady-state current using conventional PI and proposed DSR current control under reactive current variation.

demonstrates robustness under various operating conditions. The proposed strategy is validated through simulations, where it outperforms traditional PI-based control in terms of steady-state response and harmonic distortion, highlighting its potential for improving power quality and stability in real-world applications. The results illustrate that the DSR-based current controller reduces harmonic distortion and simplifies the controller design process by eliminating the need for extensive gain tuning and effectively addressing the decoupling inaccuracies. Finally, the application of DSR to generate an analytical expression for reference voltage commands is state-of-the-art in AC microgrid applications, paving the way for broader use of artificial intelligence in power conversion applications.

References

[1] M. Uddin, H. Mo, D. Dong, S. Elsawah, J. Zhu, and J. M. Guerrero, "Microgrids: A review, outstanding issues and future trends," *Energy Strategy Rev.*, vol. 49, p. 101127, 2023.

[2] A. Hirsch, Y. Parag, and J. Guerrero, "Microgrids: A review of technologies, key drivers, and outstanding issues," *Renew. Sustain. Energy Rev.*, vol. 90, pp. 402–411, 2018.

[3] M. H. Mahlooji, H. R. Mohammadi, and M. Rahimi, "A review on modeling and control of grid-connected photovoltaic inverters with LCL filter," *Renew. Sustain. Energy Rev.*, vol. 81, pp. 563–578, 2018.

[4] W. Yin and Y. Ma, "Research on three-phase PV grid-connected inverter based on LCL filter," in *Proc. IEEE 8th Conf. Ind. Electron. Appl.* IEEE, 2013, pp. 1279–1283.

[5] R. Teodorescu, F. Blaabjerg, M. Liserre, and P. C. Loh, "Proportional-resonant controllers and filters for grid-connected voltage-source converters," *IEE Proc. Elect. Power Appl.*, vol. 153, no. 5, pp. 750–762, 2006.

[6] L. Wang, T. Zhao, and J. He, "Investigation of variable switching frequency in finite control set model predictive control on grid-connected inverters," *IEEE Open J. Ind. Appl.*, vol. 2, pp. 178–193, 2021.

[7] M. A. Hannan, Z. A. Ghani, A. Mohamed, and M. N. Uddin, "Real-time testing of a fuzzy logic controller based grid-connected photovoltaic inverter system," *IEEE Trans. Ind. Appl.*, vol. 51, no. 6, pp. 4775–4784, 2015.

[8] Y. Zhang, J. Liu, and S. Fan, "On the inherent relationship between finite control set model predictive control and SVM-based deadbeat control for power converters," in *Proc. IEEE Energy Convers. Congr. Expo.* IEEE, 2017, pp. 4628–4633.

[9] S. Zhao, F. Blaabjerg, and H. Wang, "An overview of artificial intelligence applications for power electronics," *IEEE Trans. Power Electron.*, vol. 36, no. 4, pp. 4633–4658, 2021.

[10] R. Trivedi and S. Khadem, "Implementation of artificial intelligence techniques in microgrid control environment: Current progress and future scopes," *Energy and AI*, vol. 8, p. 100147, 2022.

[11] S. Zhang, O. Wallscheid, and M. Porrmann, "Machine learning for the control and monitoring of electric machine drives: Advances and trends," *IEEE Open J. Ind. Appl.*, vol. 4, pp. 188–214, 2023.

[12] B. K. Petersen, M. Landajuela, T. N. Mundhenk, C. P. Santiago, S. K. Kim, and J. T. Kim, "Deep symbolic regression: Recovering mathematical expressions from data via risk-seeking policy gradients," in *Proc. Int. Conf. Learn. Represent.*, 2021.

[13] M. Usama and I.-Y. Lee, "Data-driven non-linear current controller based on deep symbolic regression for SPMSM," *Sensors*, vol. 22, no. 21, p. 8240, 2022.

[14] E. Isen and A. F. Bakan, "Development of 10 kW three-phase grid connected inverter," *Automatika*, vol. 57, no. 2, pp. 319–328, 2016.

[15] M. Dursun and M. K. Döşoğlu, "LCL filter design for grid connected three-phase inverter," in *Proc. 2nd Int. Symp. Multidisciplinary Stud. Innov. Technol.* IEEE, 2018.

[16] M. G. Judewicz, S. A. González, J. R. Fischer, J. F. Martínez, and D. O. Carrica, "Inverter-side current control of grid-connected voltage source inverters with LCL filter based on generalized predictive control," *IEEE J. Emerg. Sel. Top. Power Electron.*, vol. 6, no. 4, pp. 1732–1743, 2018.

[17] M. Landajuela, C. S. Lee, J. Yang, R. Glatt, C. P. Santiago, I. Aravena, T. Mundhenk, G. Mulcahy, and B. K. Petersen, "A unified framework for deep symbolic regression," in *Adv. Neural Inf. Proc. Syst.*, vol. 35, 2022, pp. 33 985–33 998.

[18] D. P. Kingma and J. Ba, "Adam: A method for stochastic optimization," *arXiv preprint*, p. 1412.6980, 2014.